A peer-reviewed version of this preprint was published in PeerJ on 4 April 2018.

View the peer-reviewed version (peerj.com/articles/4603), which is the preferred citable publication unless you specifically need to cite this preprint.

Escobar-Flores JG, Lopez-Sanchez CA, Sandoval S, Marquez-Linares MA, Wehenkel C. 2018. Predicting *Pinus monophylla* forest cover in the Baja California Desert by remote sensing. PeerJ 6:e4603 https://doi.org/10.7717/peerj.4603

Predicting *Pinus monophylla* forest cover in the Baja California Desert by remote sensing

Jonathan G. Escobar-Flores [1], Carlos A. López-Sánchez [2], Sarahi Sandoval [3], Marco A. Márquez-Linares [1], Christian Wehenkel [2]

[1] Instituto Politécnico Nacional. Centro Interdisciplinario De Investigación para el Desarrollo Integral Regional, Unidad Durango., Durango, México

[2] Instituto de Silvicultura e Industria de la Madera, Universidad Juárez del Estado de Durango, Durango, México

[3] CONACYT - Instituto Politécnico Nacional. CIIDIR. Unidad Durango. Durango, México

Corresponding author:

Christian Wehenkel [2]

Km 5.5 Carretera Mazatlán, Durango, 34120 Durango, México

Email address: wehenkel@ujed.mx

ABSTRACT

Background. The Californian single-leaf pinyon (*Pinus monophylla* var. *californiarum*), a subspecies of the single-leaf pinyon (the world's only 1-needled pine), inhabits semi-arid zones of the Mojave Desert (southern Nevada and southeastern California, US) and also of northern Baja California (Mexico). This tree is distributed as a relict subspecies, at elevations of between 1,010 and 1,631 m in the geographically isolated arid Sierra La Asamblea (Baja California, Mexico), an area characterized by mean annual precipitation levels of between 184 and 288 mm. The aim of this research was i) to estimate the distribution of *P. monophylla* var. *californiarum* in Sierra La Asamblea by using Sentinel-2 images, and ii) to test and describe the relationship between the distribution of *P. monophylla* and five topographic and 18 climate variables. We hypothesized that i) Sentinel-2 images can be used to predict the *P. monophylla* distribution in

PeerJ Preprints | https://doi.org/10.7287/peerj.preprints.3439v6 | CC BY 4.0 Open Access | rec: 20 Mar 2018, publ: 20 Mar 2018

the study site due to the finer resolution (x3) and greater number of bands (x2) relative to Landsat-8 data, which is publically available free of charge and has been demonstrated to be useful for estimating forest cover, and ii) the topographical variables aspect, ruggedness and slope are particularly important because they represent important microhabitat factors that can determine the sites where conifers can become established and persist. **Methods.** An atmospherically corrected a 12-bit Sentinel-2A MSI image with ten spectral bands in the visible, near infrared, and short-wave infrared light region was used in combination with the normalized differential vegetation index (NDVI). Supervised classification of this image was carried out using a backpropagation-type artificial neural network algorithm (BPNN). Stepwise multiple linear binominal logistical regression and Random Forest classification including cross validation (10-fold) were used to model the associations between presence/absence of *P. monophylla* and the five topographical and 18 climate variables. **Results.** Using supervised classification of Sentinel-2 satellite images, we estimated that *P. monophylla* covers 6,653 ± 319 (standard error) hectares in the isolated Sierra La Asamblea. The NDVI was one of the variables that contributed most to the prediction and clearly separated the forest cover (NDVI > 0.35) from the other vegetation cover (NDVI < 0.20). Ruggedness was the most influential environmental predictor variable, indicating that the probability of occurrence of *P. monophylla* was greater than 50% when the degree of ruggedness TRI was greater than 17.5 m. The probability of occurrence of the species decreased when the mean temperature in the warmest month increased from 23.5 to 25.2 °C. **Discussion.** The accuracy of classification was similar to that reported in other studies using Sentinel-2A MSI images. Ruggedness is known to create microclimates and provides shade that minimizes evapotranspiration from pines in desert environments. Identification of the *P. monophylla* stands in Sierra La Asamblea as the most southern

PeerJ Preprints | https://doi.org/10.7287/peerj.preprints.3439v6 | CC BY 4.0 Open Access | rec: 20 Mar 2018, publ: 20 Mar 2018

populations represents an opportunity for research on climatic tolerance and community responses to climate variability and change.

INTRODUCTION

The Californian single-leaf pinyon (*Pinus monophylla* var. *californiarum*), a subspecies of the single-leaf pinyon (the world's only 1-needled pine), inhabits semi-arid zones of the Mojave Desert (southern Nevada and southeastern California, US) and also of northern Baja California (BC) (Mexico). It is both cold-tolerant and drought-resistant and is mainly differentiated from the typical subspecies *Pinus monophylla* var. *monophylla* by a larger number of leaf resin canals and longer fascicle-sheath scales (Bailey, 1987). This subspecies was first reported in BC in 1767 (Bullock et al., 2006). The southernmost record of *P. monophylla* var. *californiarum* in America was previously in BC, 26-30 miles north of Punta Prieta, at an elevation of 1,280 m (longitude -114 °.155; latitude 29 °.070, catalogue number ASU 0000235), and the type specimen is held in the Arizona State University Vascular Plant Herbarium.

This species is distributed as a relict subspecies in the geographically isolated Sierra La Asamblea, at a distance of 196 km from the Southern end of the Sierra San Pedro Martir and at elevations of between 1,010 and 1,631 m (Moran, 1983) in areas with mean annual precipitation levels of between 184 and 288 mm (Roberts & Ezcurra, 2012). The Californian single-leaf pinyon grows together with up to about 86 endemic plant species, although the number of species decreases from north to south (Bullock et al., 2008).

Adaptation of *P. monophylla* var. *californiarum* to arid ecosystems enables the species to survive annual precipitation levels of less than 150 mm. In fact, seeds of this variety survive well under

PeerJ Preprints | https://doi.org/10.7287/peerj.preprints.3439v6 | CC BY 4.0 Open Access | rec: 20 Mar 2018, publ: 20 Mar 2018

shrubs such as *Quercus spp.* and *Arctostaphylus spp.,* a strategy that enables the pines to widen their distribution, as has occurred in the great basin in California (Callaway et al., 1996; Chambers, 2001), and for them to occupy desert zones such as Sierra de la Asamblea. Despite the importance of this relict pine species, its existence is not considered in most forest inventories in Mexico (CONABIO, 2017).

Remote sensing with Landsat images has been demonstrated to be useful for estimating forest cover; the Landsat-8 satellite has sensors (7 bands) that can be predicted vegetation attributes at a spatial resolution of 30 m (Madonsela et al., 2017). However, the European Space Agency's Copernicus program has made Sentinel-2 satellite images available to the public free of charge. The spatial resolution (10 m is pixel) of the images is three times finer that of Landsat images, thus increasing their potential for predicting and differentiating types of vegetation cover (Drush et al., 2012; Borras et al., 2017). The Sentinel-2 has 13 bands, of which 10 provide greater-quality radiometric images of spatial resolution 10 to 20 m in the visible and infrared regions of the electromagnetic spectrum. These images are therefore ideal for land classification (ESA, 2017).

The aim of this research was i) to estimate the distribution of *Pinus monophylla* var. *californiarum* in Sierra La Asamblea, Baja California (Mexico) by using Sentinel-2 images, and ii) to test and describe the relationship between this distribution of *P. monophylla* and five topographic and 18 climate variables. We hypothesized that i) the Sentinel-2 images can be used to accurately predict the *P. monophylla* distribution in the study site due to finer resolution (x3) and greater number of bands (x2) than in Landsat-8 data, and ii) the topographical variables aspect, ruggedness and slope are particularly influential because they represent important

PeerJ Preprints | https://doi.org/10.7287/peerj.preprints.3439v6 | CC BY 4.0 Open Access | rec: 20 Mar 2018, publ: 20 Mar 2018

microhabitat factors that can determine where conifers can become established and persist (Marston, 2010).

MATERIALS AND METHODS

Study area

Sierra La Asamblea is located in Baja California's central desert (-114 ° 9' W 29 ° 19´ N, elevation range 280-1,662 m, Fig. 1). The climate in the area is arid, with maximum temperatures of 40 °C in the summer (Garcia, 1998). The sierra is steeper on the western slopes, with an average incline of 35 °, and with numerous canyons with occasional springs and oases. Valleys and plateaus are common in the proximity of the Gulf of California. Granite rocks occur south of the sierra and meta-sedimentary rocks along the north and southeast of the slopes. The predominant type of vegetation is xerophilous scrub, which is distributed at elevations ranging from 200 to 1,000 m. Chaparral begins at an altitude of 800 m, and representative specimens of *Adenostoma fasciculatum, Ambrosia ambrosioides, Dalea bicolor orcuttiana, Quercus tuberculata, Juniperus californica* and *Pinus monophylla* are also present at elevations above 1,000 m. Populations of the endemic palm tree *Brahea armata* also occur in the lower parts of the canyons with superficial water flow and through the rocky granite slopes (Bullock et al., 2006).

PeerJ Preprints | https://doi.org/10.7287/peerj.preprints.3439v6 | CC BY 4.0 Open Access | rec: 20 Mar 2018, publ: 20 Mar 2018

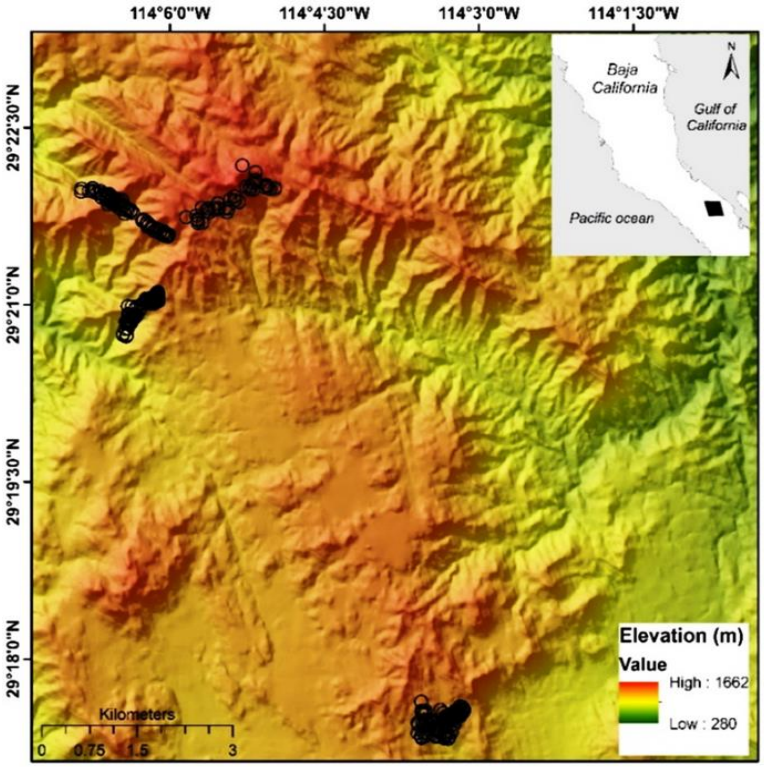

Figure 1. Map of Sierra La Asamblea. The black circles indicate georeferenced sites occupied by *Pinus monophylla*.

Datasets

Sentinel-2

The Sentinel-2A multispectral instrument (MSI) L1C dataset, acquired on 11 October 2016, in the trajectory of coordinates latitude 29 °.814, longitude 114 °.93, was downloaded from the US. Geological Survey (USGS) Global Visualization Viewer at http://glovis.usgs.gov/. The 12-bit Sentinel-2A MSI image has 13 spectral bands in the visible, NIR, and SWIR wavelength regions with spatial resolutions of 10-60 m. However, band one, used for studies of coastal aerosols, and bands nine and ten, applied for respectively water vapour correction and cirrus detection, were not used in this study (ESA, 2017). Hence, the data preparation involved four bands at 10 m and

PeerJ Preprints | https://doi.org/10.7287/peerj.preprints.3439v6 | CC BY 4.0 Open Access | rec: 20 Mar 2018, publ: 20 Mar 2018

126 the resampling of the six S2 bands acquired at 20 m to obtain a layer stack of 10 spectral bands at
127 10 m (Table 1) using the ESA´s Sentinel-toolbox ESA Sentinel Application Platform (SNAP)
128 and then converted to ENVI format.

129 Because atmospherically improved images are essential to enable assessment of spectral indices
130 with spatial reliability and product comparison, Level-1C data were converted to Level-2A
131 (Bottom of Atmosphere -BOA- reflectance) by taking into account the effects of aerosols and
132 water vapour on reflectance (Radoux et al., 2016). The corrections were made using the Sen2Cor
133 tool (Telespazio VEGA Deutschland GmbH, 2016) for Sentinel-2 images.

134 **Table 1.** Sentinel-2 spectral bands used to predict the *Pinus monophylla* forest cover

Band	Central wavelength (µm)	Resolution (m)
Band 2–Blue	0.490	10
Band 3 –Green	0.560	10
Band 4 – Red	0.665	10
Band 5- Vegetation red edge	0.705	20
Band 6– Vegetation red edge	0.740	20
Band 7– Vegetation red edge	0.783	20
Band 8- NIR	0.842	10
Band 8A– Vegetation red edge	0.865	20
Band 11 –SWIR	1.610	20
Band 12 –SWIR	2.190	20

135

136 The following equation was used to calculate the normalized difference vegetation index
137 (NDVI): NDVI = (NIR – R) / (NIR + R), where NIR is the near infrared light (band) reflected by
138 the vegetation, and R is the visible red light reflected by the vegetation (Rouse et al., 1974). The
139 NDVI is useful for discriminating the layers of temperate forest from scrub and chaparral. Areas
140 occupied by large amounts of unstressed green vegetation will have values much greater than 0

PeerJ Preprints | https://doi.org/10.7287/peerj.preprints.3439v6 | CC BY 4.0 Open Access | rec: 20 Mar 2018, publ: 20 Mar 2018

and areas with no vegetation will have values close to 0 and, in some cases, negative values (Pettorelli, 2013). The NDVI image was combined with the previously described multi spectral bands.

Environmental variables

Tree species distribution is generally modulated by hydroclimate and topographical variables (Elliot et al., 2005; Decastilho et al., 2006), which can be estimated from digital terrain models (DTM) (Osem et al., 2005; Spasojevic et al., 2016). A DTM was obtained by using tools available from the Instituto Nacional de Estadistica y Geografía (http:www.inegi.org.mx/geo/contenidos/datosrelieve) with a spatial resolution of 15 m. The DTM was processed with the QGIS (QGIS Development Team, 2016), using *Terrain analysis* tools, elevation, slope and aspect (Table 2).

The ruggedness was estimated using two indexes: i) the terrain ruggedness index (TRI) of Riley et al. (1999) and ii) a vector ruggedness measure (VRM), both implemented in QGIS (QGIS Development Team, 2016). The TRI computes the values for each grid cell of a DEM. This calculates the sum change in elevation between a grid cell and its eight-neighbor grid cell. VRM incorporates the heterogeneity of both slope and aspect. This measure of ruggedness uses 3-dimensional dispersion of vectors normal to planar facets on landscape. This index lacks units and ranges from 0 (indicating a totally flat area) to 1 (indicating maximum ruggedness) (Sappington et al., 2007).

In addition, 18 climate variables with a 30-arc second resolution (approximate 800 meters) (Table 2) were obtained from a national database managed by the University of Idaho (http://charcoal.cnre.vt.edu/climate) and which requires point coordinates (latitude, longitude and

PeerJ Preprints | https://doi.org/10.7287/peerj.preprints.3439v6 | CC BY 4.0 Open Access | rec: 20 Mar 2018, publ: 20 Mar 2018

elevation) as the main inputs (Rehfeldt, 2006; Rehfeldt et al., 2006). These variables are frequently used to study the potential effects of global warming on forests and plants in Western North America and Mexico (Sáenz-Romero et al., 2010; Silva-Flores et al., 2014).

Table 2. Topographical and climatic variables considered in the study

Variable	Abbreviation	Units	Mean	SD	Max	Min
Ruggedness	IRT	m	20.33	6.66	35.90	4.69
Ruggedness VRM	VRM	NA	0.005	0.007	0.13	0
Slope	S	º	28.38	8.92	48.34	3.42
Aspect *	A	º	190.51	68.72	350.44	20.55
Elevation *	E	m	1302.41	124.96	1631	1010
Mean annual temperature *	MAT	°C	16.57	0.38	17.4	15.5
Mean annual precipitation *	MAP	mm	229.56	19.95	288	184
Growing season precipitation, April-September *	GSP	mm	79.08	9.60	108	57
Mean temperature in the coldest month *	MTCM	°C	10.85	0.37	11.7	9.8
Minimum temperature in the coldest month *	MMIN	°C	3.42	0.41	4.3	2.3
Mean temperature in the warmest month	MTWM	°C	24.52	0.31	25.2	23.5
Maximum temperature in the warmest month	MMAX	°C	34.10	0.31	34.7	33.1
Julian date of the last freezing data of spring *	SDAY	Days	82.57	7.86	106	60
Julian date of the first freezing data of autumn *	FDAY	Days	331.28	2.62	339	324
Length of the frost-free period *	FFP	Days	259.22	8.36	285	240
Degree days > 5°C *	DD5	Days	4245.26	137.52	4550	3852
Degree days > 5°C accumulating within the frost-free period *	GSDD5	Days	3491.82	164.76	3944	2995
Julian date when the sum degree days > 5°C reaches 100 *	D100	Days	17.07	1.10	20	15
Degree days < 0 °C *	DD0	Days	0	0	0	0
Minimum degree days < 0 °C *	MMINDD0	Days	8.07	20.29	145	45
Spring precipitation	Sprp	mm	7.54	0.71	10	6
Summer precipitation *	Smrp	mm	43.74	6.29	62	29
Winter precipitation *	Winp	mm	110.93	7.93	133	93

PeerJ Preprints | https://doi.org/10.7287/peerj.preprints.3439v6 | CC BY 4.0 Open Access | rec: 20 Mar 2018, publ: 20 Mar 2018

* Variables for which no significant difference between the medians was obtained after Bonferroni correction ($\alpha = 0.0005$) were excluded from further analysis.

Pixel-based classification

Classification method

Pixel-based classification was carried out in order to predict four different types of land cover in the study area (*P. monophylla*, scrub, chaparral and no apparent vegetation). A supervised classification approach with a backpropagation-type artificial neural network (BPNN) (Tan and Smeins, 1996) was applied. BPNN is widely used because of its structural simplicity and robustness in modelling non-linear relationships. In this study, the BPNN comprises a set of three layers (raster): an input layer, a hidden layer and an output layer (Richards, 1999). Each layer consists of a series of parallel processing elements (neurons or nodes). Each node in a layer is linked to all nodes in the next layer (Guo et al., 2013).

The first step in BPNN supervised classification is to enter the input layer, which in this study corresponded to the values of the pixels of ten Sentinel-2 bands and of the NDVI image. Weights were then assigned to the BPNN to produce analytical predictions from the input values. These data were contrasted with the category to which each training pixel belongs, corresponding to Georeferenced sites (Datum WGS-84, 11N) obtained in the field in October 2014 and October 2015.

A stratified random sampling method (Olofsson et al., 2013) was used to generate the reference data in QGIS software (QGIS Development Team, 2016). A total of 2143 random points were sampled, with at least 400 points for each class (Goodchild et al., 1994). The following classes were considered: i) *P. monophylla*, 536 sites, ii) scrub, 764 sites, iii) chaparral, 405 sites, and iv)

PeerJ Preprints | https://doi.org/10.7287/peerj.preprints.3439v6 | CC BY 4.0 Open Access | rec: 20 Mar 2018, publ: 20 Mar 2018

no apparent vegetation, 438 sites. Class discrimination processes occurred in the hidden layer and the synapses between the layers were estimated by an activation function. We used a logistic function and training rate of 0.20, previously applied to land cover classification (Hepner et al., 1990; Richards, 1999; Braspenning & Thuijisman, 1995). Learning occurs by adjusting the weights in the node to minimize the difference between the output node activation, and BPNN then calculates the error at each iteration with root mean square error (RMS). The output layer comprised four neurons representing the four target classes of land cover (*P. monophylla*, Scrub, Chaparral and no apparent vegetation). Average spectral signatures for the four different types of land cover are shown in Figure 2.

Figure 2. Average spectral signatures of cover vegetation in Sierra La Asamblea, Baja California.

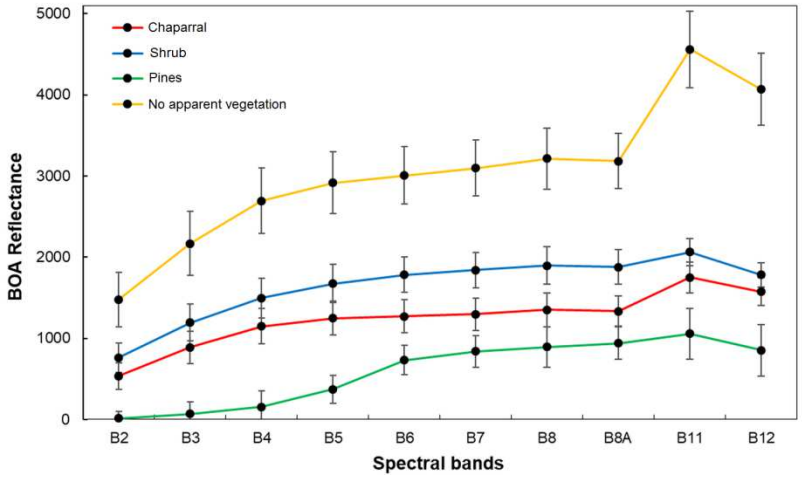

Validation

The BPNN classification was cross-validated (10-fold) using a confusion matrix, which is a table that compares the reference data and the classification results. We estimated the uncertainty of the classification using estimated error matrix in terms of proportion of area and estimates of

PeerJ Preprints | https://doi.org/10.7287/peerj.preprints.3439v6 | CC BY 4.0 Open Access | rec: 20 Mar 2018, publ: 20 Mar 2018

overall map accuracy ($\widehat{O}$), user's accuracy ($\widehat{U}_i$) (or commission error) and producer's accuracy ($\widehat{P}_j$) (or omission error) recommended by Olofsson et al. (2013): p_{ij} is defined as a cell entry of error matrix of i map classes. A poststratified estimator of p_{ij} is:

$$\hat{p}_{ij} = W_i \frac{n_{ij}}{n_{i.}} \tag{1}$$

where W_i is the proportion of the area mapped as class i. $n_{i.}$ is the total number of sample units in map class i. n_{ij} is the sample count at cell (i,j) in the error matrix.

$\hat{p}_{.j}$ is a poststratified estimator for simple random and systematic sampling:

$$\hat{p}_{.j} = \sum_{i=1}^{q} W_i \frac{n_{ij}}{n_{i.}} \tag{2}$$

where q is the class number.

An unbiased estimator of the total area of class j is then

$$\hat{A}_j = A \cdot \hat{p}_{.j} \tag{3}$$

where A is the total map area. For $\hat{p}_{.j}$, the standard error is estimated by:

$$S(\hat{p}_{.j}) = \sqrt{\sum_{i=1}^{q} W_i^2 \frac{\frac{n_{ij}}{n_{i.}}\left(1 - \frac{n_{ij}}{n_{i.}}\right)}{n_{i.} - 1}} \tag{4}$$

The standard error of the error-adjusted estimated area is

$$S(\hat{A}_j) = A \cdot S(\hat{p}_{.j}) \tag{5}$$

Finally,

$$\hat{A}_j \pm 1.96 \cdot S(\hat{A}_j) \tag{6}$$

presents an approximate 95% confidence interval.

PeerJ Preprints | https://doi.org/10.7287/peerj.preprints.3439v6 | CC BY 4.0 Open Access | rec: 20 Mar 2018, publ: 20 Mar 2018

The $\hat{O}$, $\hat{U}_i$ and $\hat{P}_j$ were calculated with Eqs. (7-9) (Congalton, 1991). $\hat{U}_i$ of class i is the proportion of the area mapped as class i that has reference class i. $\hat{P}_j$ of class j is the proportion of the area of reference class j that is mapped as class j.

$$\hat{O} = \sum_{j=1}^{q} \hat{p}_{jj} \tag{7}$$

$$\hat{U}_i = \frac{\hat{p}_{ii}}{\hat{p}_{i.}} \tag{8}$$

$$\hat{P}_j = \frac{\hat{p}_{jj}}{\hat{p}_{.j}} \tag{9}$$

We then generated a map from the results of the probability of class assignment. The accuracy of classification was also estimated using the Kappa (K) coefficient. The K coefficient is often used as an overall measure of accuracy (Abraira, 2001). This coefficient takes values of between 0 and 1, where values close to one indicate a greater degree of agreement between classes and observations, and a value of 0 suggests that the observed agreement is random. However, the use of K is controversial because i) K would underestimate the probability that a randomly selected pixel is correctly classified, ii) K is greater correlated with overall accuracy so reporting Kappa is redundant for overall accuracy (Olofsson et al., 2014).

Relationship between presence of *P. monophylla* and environmental variables

To model and test the association between presence/absence of *P. monophylla* in the study area and topographical or climate variables, a Kruskal-Wallis test was used to estimate the difference in the median values in relation to presence and absence of *P. monophylla*. All variables for which no significant difference between the median values was predicted after Bonferroni

PeerJ Preprints | https://doi.org/10.7287/peerj.preprints.3439v6 | CC BY 4.0 Open Access | rec: 20 Mar 2018, publ: 20 Mar 2018

correction (α = 0.0005) were excluded from further analysis. The collinearity between the variables with a significant difference between the medians of presence and absence was estimated using the Spearman correlation coefficient (r_s). When the r_s value for the difference between two variables was greater than 0.7, only the variable with the lowest p value in the Kruskal-Wallis test was used in the models (as reported by Salas et al., 2017 and Shirk et al., 2018). Finally, stepwise multiple linear binominal logistical regression and Random Forest classification including cross valuation (10-fold) were used to model the associations between presence/absence of *P. monophylla* and the most important topographical and climate variables (Shirk et al., 2018).

Regression and classification including cross-validations were carried out using the trainControl, train, glm (family = "binomial") and rf functions, as well as the "randomForest" and "caret" packages (Venables and Ripley, 2002) in R (version 3.3.2) (Development Core Team, 2017). The goodness-of-fit of the logistical regression model was evaluated using the Akaike information criterion (AIC), root-mean-square error (RMSE) and residual deviance. Validation of the randomForest model was performed using under the curve (AUC; Fawcett, 2006), True Skill Statistic (TSS; Allouche et al., 2006), Kappa (Abraira, 2001), specificity and sensitivity.

RESULTS

Pixel-based classification

We estimated the area of *P. monophylla* cover with a margin of error (at approximate 95% confidence interval) of 6,653 ± 319 (standard error) hectares in Sierra de la Asamblea, Baja California, Mexico (Fig. 3). The confusion matrix of the accuracy assessment is listed in Table 3 including user´s and producer´s accuracy for each class. The supervised classification with

PeerJ Preprints | https://doi.org/10.7287/peerj.preprints.3439v6 | CC BY 4.0 Open Access | rec: 20 Mar 2018, publ: 20 Mar 2018

BPNN yielded predictions with an overall accuracy of identification of 87.74% (Table 4). This level of accuracy was estimated in the 32 interactions with 0.04 RMS training. The proportion of omission errors in the *P. monophylla* class was only 2.62%, *i.e.* 97.39% of the pixels were correctly classified. The shrub class had the larger proportion of omission errors (18.98%). The value of NDVI in the *P. monophylla* forest fluctuated between 0.30 and 0.41, and in chaparral between 0.24 and 0.28. The smallest values of NDVI corresponded to scrub vegetation, with values between 0.10 and 0.15.

Figure 3. (A) Estimated land cover classes using BPNN classification in Sierra La Asambla. (B) Probability map of class assignment.

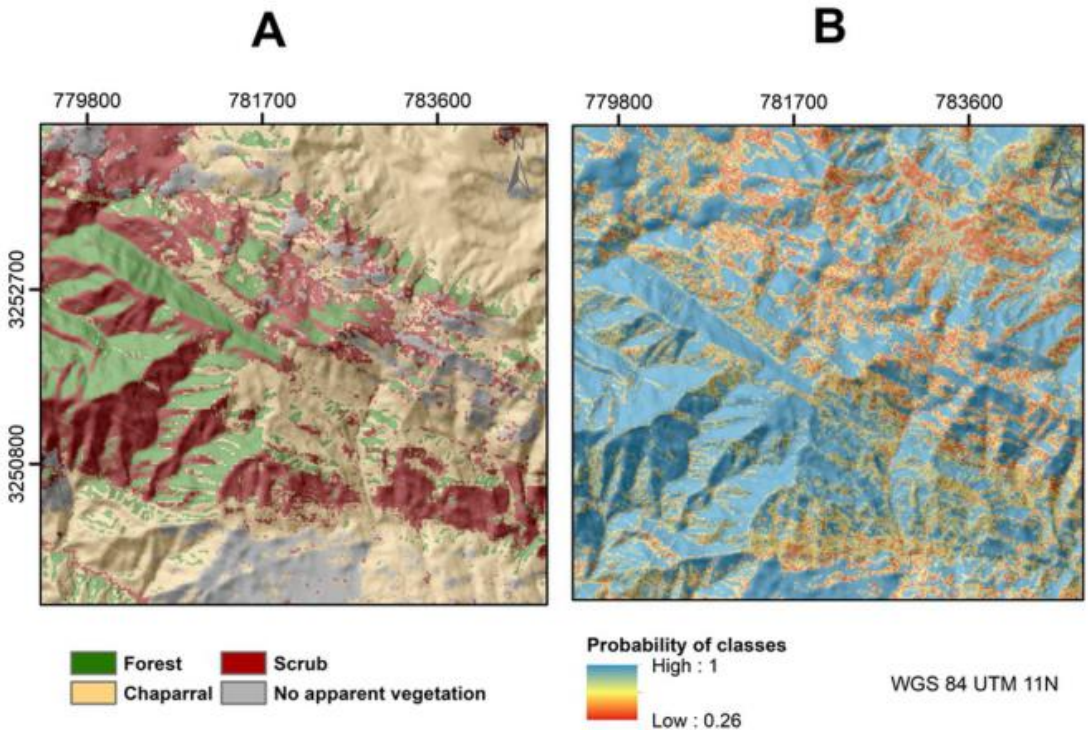

PeerJ Preprints | https://doi.org/10.7287/peerj.preprints.3439v6 | CC BY 4.0 Open Access | rec: 20 Mar 2018, publ: 20 Mar 2018

269 **Table 3**. Estimated error matrix based of sample counts (n_{ij}) from the accuracy assessment
270 sample. Map classes are the rows while the reference classes are the columns

		Reference				Total	Map area (ha)	W_i
	Classes*	**P**	**S**	**C**	**WV**			
Map	**P**	522	0	14	0	536	5,395	0.169
	S	24	619	119	2	764	12,309	0.387
	C	50	0	348	7	405	8,206	0.258
	WV	0	0	20	418	438	5,913	0.186
	Total	596	619	501	427	2,143	31,823	1

271 * Classes: P = *Pinus monophylla*; S = shrub; C = chaparral; WV= without vegetation; W_i =
272 proportion of the area mapped as class *i*.
273

274 **Table 4**. Error matrix of four classes with cell entries (p_{ij}) based on Table 3 and expressed in
275 terms of proportion of area. Accuracy measures are presented with a 95% confidence interval.
276 Map classes (rows), reference classes (columns).

		References				Accuracy		
	Classes	**P**	**S**	**C**	**WV**	**User´s**	**Producer´s**	**Overall**
Map	**P**	0.1651	0.0000	0.0044	0.0000	0.970±0.07	0.790±0.04	0.877±0.01
	S	0.0122	0.3134	0.0602	0.0010	0.810±0.02	1.000	
	C	0.0318	0.0000	0.2216	0.0045	0.859±0.01	0.752±0.07	
	WV	0.0000	0.0000	0.0085	0.1773	0.954±0.002	0.970±0.02	
	Total	0.2091	0.3134	0.2947	0.1828			

277

278

PeerJ Preprints | https://doi.org/10.7287/peerj.preprints.3439v6 | CC BY 4.0 Open Access | rec: 20 Mar 2018, publ: 20 Mar 2018

279 **Relationship between presence of *P. monophylla* and environmental variables**

280 The Kruskal-Wallis test indicated that the median values for ruggedness TRI ($p < 2.1x10^{-16}$),
281 slope ($p < 2.2x10^{-16}$), ruggedness VRM ($p = 4.9x10^{-9}$), MTWM ($p = 0.000014$), MMAX ($p =$
282 0.000048) and SPRP ($p = 0.00037$) were most variable between sites in which *P. monophylla*
283 was present and absent. The variable slope was closely correlated with ruggedness as well as
284 with MMAX and MTWM ($r_s > 0.7$). The p_{slope} of the Kruskal-Wallis test was larger than
285 $p_{ruggedness}$ and p_{MMAX} was larger than p_{MTWM}. Slope and MMAX were therefore excluded from the
286 model analysis. The stepwise multiple linear binominal logistical and Random Forest models
287 showed that the "presence of *P. monophylla*" model included the independent variables
288 ruggedness, ruggedness VRM and average temperature in the warmest month (MTWM) (Table
289 5).

290 The ruggedness factor was the most influential predictor variable and indicated that the
291 probability of *P. monophylla* occurrence was larger than 50% when the degree of ruggedness
292 TRI was greater than 17.5 m (Table 5). The ruggedness VRM also indicated that a minimum
293 change in roughness increases the probability of presence of the pine. The probability of
294 occurrence of *Pinus monophylla* decreased when MTWM increased from 23.5 to 25.2 °C (Table
295 5). After cross validation (10-fold), the Random Forest model revealed that the variables
296 ruggedness TRI, ruggedness VRM and MTWM yielded a greater correlation for their ability to
297 predict presence of the *P. monophylla* (AUC = 0.920, TSS = 0.690, Kappa = 0.691). The
298 sensitivity was 0.812 and specificity was 0.878.

PeerJ Preprints | https://doi.org/10.7287/peerj.preprints.3439v6 | CC BY 4.0 Open Access | rec: 20 Mar 2018, publ: 20 Mar 2018

Table 5. Results of the multiple linear binomial logistic regression model (AIC = 601.8; residual deviance= 593.85 on 588 degrees of freedom), TRI = terrain ruggedness index, VRM = vector ruggedness measure, MTWM = mean temperature in the warmest month.

Variable	Estimate	Std. Error	Z value	Pr(>|z|)
Intercept	25.351	8.895	2.850	0.0044
MTWM	-1.159	0.362	-3.201	0.0014
Roughness TRI	0.178	0.015	11.200	< 2e-16
Roughness VRM	28.476	13.847	2.056	0.0397

DISCUSSION

Pixel-based classification

Predicting the presence of pine forest by using BPNN proved feasible. The NDVI was one of the variables that contributed to the prediction and clearly separated forest cover (NDVI > 0.35) from the other types of vegetation cover (NDVI < 0.20). The overall accuracy of classification (K = 0.87) was similar to that reported in other studies using Sentinel-2A MSI images. For example, Immitzer et al. (2016) reported a K of 0.85 for tree prediction in Europe by using five classes and a random forest classifier. Vieira et al. (2003) reported a K = 0.77 in eastern Amazon using seven classes and 1999 Landsat 7 ETM imagery. However, Sothe et al. (2017) reported K values of 0.98 and 0.90 for respectively three successional forest stages and field in a subtropical forest in Southern Brazil by using Sentinel-2 and Landsat-8 data associated with the support vector machine algorithm. Kun et al. (2014) estimated K values of 0.70 to 0.85 for land-use type prediction (including forest) in China by using the support vector machine algorithm classifier

PeerJ Preprints | https://doi.org/10.7287/peerj.preprints.3439v6 | CC BY 4.0 Open Access | rec: 20 Mar 2018, publ: 20 Mar 2018

317 and Landsat-8 images of rougher spatial resolution than Sentinel images. The very greater
318 accuracy of predictions by Kun et al. (2014) was probably due to the large-scale of the study and
319 the clearly differentiated types of land considered.

320 **Relationship between presence of *P. monophylla* and environmental variables**

321 Ruggedness of the terrain was the most important topographic variable, significantly explaining
322 the presence of pines in Sierra La Asamblea (Table 5). Ruggedness, which is strongly positively
323 correlated with slope, may reduce solar radiation, air temperature and evapotranspiration due to
324 increased shading (Tsujino et al., 2006; Bullock et al., 2008). The ruggedness indicated by the
325 TRI index explains the presence of the pines because Sierra La Asamblea is heterogeneous in
326 terms of elevation. The VRM index was less important partly because the index is strongly
327 dependent on the vector aspect (Gisbert & Martí, 2010) and in the case of Sierra Asamblea the
328 aspect is very homogeneous and the index values therefore tend to be very low (Table 5), as also
329 reported by Wu et al. (2018). The pines were expected to colonize north facing slopes, which are
330 exposed to less solar radiation than slopes facing other directions. However, the topographical
331 variable aspect was not important in determining the presence of *P. monophylla* var.
332 *californiarum* in the study site, possibly because of physiological adaptations regarding water-
333 use efficiency and photosynthetic nitrogen-use efficiency (DeLucia & Schlesinger, 1991), as
334 reported for the *Pinus monophylla, P. halepensis, P. edulis* and *P. remota* in arid zones (Lanner
335 & Van Devender, 2000; Helman et al., 2017). The Mediterranean climate, with wet winters and
336 dry summers, is another characteristic factor in this mountain range. In the winter in this part of
337 the northern hemisphere, the sun (which is in a lower position and usually affects the southern
338 aspect by radiation) is masked by clouds, rainfall and occasional snowfall (León-Portilla, 1988).

PeerJ Preprints | https://doi.org/10.7287/peerj.preprints.3439v6 | CC BY 4.0 Open Access | rec: 20 Mar 2018, publ: 20 Mar 2018

339 During the summer, the solar radiation is more intense, but similar in all directions because the
340 sun is closest to its highest point (Stage & Salas, 2007).

341 The above-mentioned finding contrasts with those of other studies reporting that north-eastern
342 facing slopes in the northern hemisphere receive less direct solar radiation, thus providing more
343 favourable microclimatic conditions (air temperature, soil temperature, soil moisture) for forest
344 development, permanence and productivity than southwest-facing sites (Astrom et al., 2007;
345 Stage & Salas, 2007; Hang et al 2009; Marston et al., 2010; Klein et al., 2014). DeLucia &
346 Schleinger (1991) reported that *P. monophylla* populations in the Great Basin California desert
347 with summer rainfall (monsoon) preferred an east-southeast aspect with less intense solar
348 radiation and evapotranspiration.

349 The probability of occurrence of *P. monophylla* was also related to the climatic variable MTWM.
350 In Sierra La Asamblea, this pine species was found in a narrow range of MTWM of between
351 23.5° and 25.2° (Table 1), which, however, is a smaller range than reported for the other pine
352 species (Tapias et al., 2004; Roberts & Ezcurra, 2012). Therefore, this species should adapt well
353 to greater temperatures in the summer (Lanner et al., 2000), which is usually a very dry period in
354 the study site (León-Portilla, 1988). However, the probability of occurrence was greatest for an
355 MTWM of 23.5 °C (Table 5), which occurred at the top of Sierra La Asamblea, at an elevation
356 of about 1,660 m). We therefore conclude that this species can also grow well when the MTWM
357 is below 23.5 °C. On the other hand, considering MTWM as factor yielded a probability of
358 occurrence of 25-80%. The spatial resolution of the climatic data by the national database run by
359 the University of Idaho is probably not adequate for describing the microhabitat of *P.*
360 *monophylla* (Rehfeldt et al., 2006; Marston et al., 2010).

PeerJ Preprints | https://doi.org/10.7287/peerj.preprints.3439v6 | CC BY 4.0 Open Access | rec: 20 Mar 2018, publ: 20 Mar 2018

Identification of the *P. monophylla* stands in Sierra La Asamblea as the most southern populations represents an opportunity for research on climatic tolerance and community responses to climatic variation and change.

ACKNOWLEDGEMENTS

We are grateful to E. Espinoza, F. Macias and A. Guerrero for support with the fieldwork.

REFERENCES

Abraira V. 2001. El índice kappa. *Semergen* 27:247-249. DOI:10.1016/S1138- 3593(01)73955-X

Allen CD, Macalady AK, Chenchouni H, Bachelet D, Vennetier M, Kitzberger G, Rigling H, Breshears D, Hoog T, Gonzalez PK., Fensham R, Zhangm Z, Castro J, Demidova N, Jong-Hwan L, Allard G, Running S, Semerci A, Cobbt N. 2010. A global overview of drought and heat-induced tree mortality reveals emerging climatic change risks for forest. *Forest ecology and management* 259:660-684. DOI: 10.1016/j.foreco.2009.09.001.

Allouche, O., Tsoar, A., Kadmon, R., 2006. Assessing the accuracy of species distribution models: Prevalence, kappa and the true skill statistic (TSS). J. Appl. Ecol. 43, 1223–1232. DOI:10.1111/j.1365-2664.2006.01214.x

Bailey DK. 1987. A study of *Pinus* subsection *Cembroides*. The single-needle pinyons of the Californias and the Great Basin. Notes from the Royal Botanic Garden, Edinburgh. 44:275-310.

379 Borràs J, Delegido J, Pezzola A, Pereira M, Morassi G, Camps-Valls G. 2017. Land use
380 classification from Sentinel-2 imagery. *Revista de Teledetección* 48:55-66. DOI:
381 10.4995/raet.2017.7133.

382 Braspenning P J, Thuijsman F. 1995. Artificial neural networks: an introduction to ANN theory
383 and practice. Springer Science & Business Media. USA. 295 p.

384 Brockmann Consult, 2017. Sentinel Application Platform (SNAP). Available at:
385 http://step.esa.int/main. / (accessed 18 April 2017).

386 Bullock SH, Heath D. 2006. Growth rates and age of native palms in the Baja California desert.
387 *Journal of Arid Environments* 67(3):391-402. DOI: 10.1016/j.jaridenv.2006.03.002.

388 Bullock SH, Salazar Ceseña JM, Rebman JP, Riemann H. 2008. Flora and vegetation of an
389 isolated mountain range in the desert of Baja California. *The Southwestern Naturalist*
390 53:61-73. DOI: 10.1894/0038-4909(2008)53[61:FAVOAI]2.0.CO;2.

391 Callaway RM, DeLucia EH, Nowak R, Schlesinger WH. 1996. Competition and facilitation:
392 contrasting effects of *Artemisia tridentata* on desert vs. montane pines. *Ecology* 77:2130-
393 2141. DOI: 10.2307/2265707.

394 Chambers JC. 2001. *Pinus monophylla* establishment in an expanding *Pinus-Juniperus*
395 woodland: Environmental conditions, facilitation and interacting factors. *Journal of*
396 *Vegetation Science* 12:27-40.

397 Cochran, W. G., 1977. Sampling techniques. New York, NY: Wiley.

PeerJ Preprints | https://doi.org/10.7287/peerj.preprints.3439v6 | CC BY 4.0 Open Access | rec: 20 Mar 2018, publ: 20 Mar 2018

CONABIO. 2017. Comisión Nacional para el Conocimiento y uso de la Biodiversidad. Geoportal de información. Sistema Nacional de información sobre Biodiversidad. *Available at*: http://www.conabio.gob.mx/informacion/gis/ (accessed 12 February 2017).

Congalton RG. 1991. A review of assessing the accuracy of classifications of remotely sensed data. Remote sensing of environment 37:35-46. DOI: 10.1016/0034-4257(91)90048-B

DeCastilho CV, Magnusson WE, de Araújo RNO, Luizao RC, Luizao FJ, Lima AP, Higuchi N. 2006. Variation in aboveground tree live biomass in a central Amazonian Forest: Effects of soil and topography. *Forest ecology and management* 234:85-96. DOI: 10.1016/j.foreco.2006.06.024.

DeLucia, EH, & Schlesinger, WH. 1991. Resource- use efficiency and drought tolerance in adjacent Great Basin and sierran plants. *Ecology*, *72*(1), 51-58. DOI: 10.2307/1938901

Development Core Team. 2017. A language and environment for statistical computing. R foundation for statistical computing, Vienna Austria. *Available at*: http://www.R-project.org. (accessed 8 September 2017).

Drusch M, Del Bello U, Carlier S, Colin O., Fernández V, Gascón F, Hoersch B, Isola C, Laberinti, P, Martimort P, Meygret A, Spoto F, Sy O, Marchese F, Bargellini P. 2012. Sentinel-2: ESA's Optical High-Resolution Mission for GMES Operational Services. *Remote sensing environment* 120:25-36. DOI: 10.1016/j.rse.2011.11.026.

PeerJ Preprints | https://doi.org/10.7287/peerj.preprints.3439v6 | CC BY 4.0 Open Access | rec: 20 Mar 2018, publ: 20 Mar 2018

Elliott KJ, Miniat CF, Pederson N, Laseter SH. 2005. Forest tree growth response to hydroclimate variability in the southern Appalachians. *Global Change Biology* 21(12):4627-4641. DOI: 10.1111/gcb.13045.

ESA, 2017. European Space Agency. Copernicus, Sentinel-2. *Available At*: http://www.esa.int (accessed 21 March 2016).

Fawcett, T. 2006. An introduction to ROC analysis. Pattern Recognition Letters 27:861–874. DOI: 10.1016/j.patrec.2005.10.010

García E. 1998. Clasificación de Köppen, modificado por García, E. Comisión Nacional para el Conocimiento y Uso de la Biodiversidad (CONABIO), 1998. Available at: http://www.conabio.gob.mx/informacion/gis/ (accessed 2 June 2017).

Gisbert FJG, Martí IC. 2010. Un índice de rugosidad del terreno a escala municipal a partir de Modelos de Elevación Digital de acceso público. *Documento de Trabajo*. Available at: https://wheui3.grupobbva.com/TLFU/dat/DT_7_2010.pdf

Goodchild MF. 1994. Integrating GIS and remote sensing for vegetation analysis and modeling: methodological issues. *Journal of Vegetation Science* 5:615-626. DOI: 10.2307/3235878.

Guo PT, Wu W, Sheng QK, Li MF, Liu HB, Wang ZY. 2013. Prediction of soil organic matter using artificial neural network and topographic indicators in hilly areas. *Nutrient cycling in agroecosystems* 95:333344. DOI: 10.1007/s10705-013-9566-9.

Helman D, Osem Y, Yakir D, Lensky IM. 2017. Relationships between climate, topography, water use and productivity in two key Mediterranean forest types with different water-use

PeerJ Preprints | https://doi.org/10.7287/peerj.preprints.3439v6 | CC BY 4.0 Open Access | rec: 20 Mar 2018, publ: 20 Mar 2018

436 strategies. *Agricultural and Forest Meteorology* 232:319-330. DOI:
437 10.1016/j.agrformet.2016.08.018.

438 Hepner G, Logan T, Ritter N, Bryant N. 1990. Artificial neural network classification using a
439 minimal training set. Comparison to conventional supervised classification.
440 *Photogrammetric Engineering and Remote Sensing* 56(4):469-473.

441 Immitzer M,Vuolo F, Atzberger C. 2016. First Experience with Sentinel-2 Data for Crop and
442 Tree Species Classifications in Central Europe. *Remote Sensing* 8:1-27. DOI:
443 10.3390/rs8030166.

444 INEGI. 2013. Conjunto de datos vectoriales de uso de suelo y vegetación escala 1:250 000, serie
445 V. Instituto Nacional de Estadística y Geografía. Aguascalientes. *Available at*:
446 http://www.conabio.gob.mx/informacion/gis/ (accessed 10 September 2015).

447 Klein T, Hoch G, Yakir D, Körner C. 2014. Drought stress, growth and nonstructural
448 carbohydrate dynamics of pine trees in a semi-arid forest. *Tree physiology* 34:981-992.
449 DOI: 10.1093/treephys/tpu071.

450 Kun J, Xiangqin W, Xingfa G, Yunjun J. Xianhong X, Bin L. 2014. Land cover classification
451 using Landsat 8 Operational Land Imager data in Beijing, China. *Geocarto International*
452 29:941-951. DOI:10.1080/10106049.2014.894586.

453 Lanner RM, Van Devender TR. 2000. The recent history of pinyon pines. In: Richardson, D. M.
454 (eds). The American Southwest, Cambridge University Press. 171–182

455 Léon-Portilla. 1988. Miguel del Barco, Historia natural y crónica de la antigua California.
456 Universidad Nacional Autónoma de México, México. 483 p.

457 Madonsela S, Cho MA., Ramoelo A, Mutanga O. 2017. Remote sensing of species diversity
458 using Landsat 8 spectral variables. *ISPRS Journal of Photogrammetry and Remote Sensing*
459 133: 116–127. DOI: 10.1016/j.isprsjprs.2017.10.008.

460 Marston, RA. 2010. Geomorphology and vegetation on hillslopes: interactions, dependencies,
461 and feedback loops. *Geomorphology*, *116*(3-4), 206-217.

462 Moran RV. 1983. Relictual northern plants on peninsular mountain tops. In: Biogeography of the
463 Sea of Cortez; University of California Press, Berkeley, USA. 408–410.

464 Olofsson O, Foody GM, Stehman SV, Woodcock CE. 2013. Making better use of accuracy data
465 in land change studies: Estimating accuracy and area and quantifying uncertainty using
466 stratified estimation. *Remote Sensing of Environment* 129:122–131. DOI:
467 10.1016/j.rse.2012.10.031

468 Olofsson, P, Foody, GM, Herold, M, Stehman, SV, Woodcock, CE, Wulder, MA. 2014. Good
469 practices for estimating area and assessing accuracy of land change. *Remote Sensing of*
470 *Environment* 148, 42-57. DOI: 10.1016/j.rse.2014.02.015

471 Osem Y, Zangy E, Bney-Moshe E., Moshe Y, Karni N, Nisan Y. 2009. The potential of
472 transforming simple structured pine plantations into mixed Mediterranean forests through
473 natural regeneration along a rainfall gradient. *Forest Ecology Management* 259:14–23.
474 DOI:10.1016/j.foreco.2009.09.034.

PeerJ Preprints | https://doi.org/10.7287/peerj.preprints.3439v6 | CC BY 4.0 Open Access | rec: 20 Mar 2018, publ: 20 Mar 2018

475 Pettorelli N. 2013. The Normalized Difference Vegetation Index. Oxford, University Press.
476 United Kingdom. 194 p.

477 QGIS Development, 2016. QGIS Geographic Information System. Open source Geospatial
478 Foundation. Available at: http//qgis.osgeo.org

479 Radoux J, Chomé G, Jacques DC, Waldner F, Bellemans N, Matton N, Lamarche C,
480 d'Andrimont R, Defourny P. 2016. Sentinel-2's potential for sub-pixel landscape feature
481 detection. *Remote Sensing* 8(6):488. DOI:10.3390/rs8060488.

482 Rehfeldt GE, 2006. A spline model of climate for the Western United States. Gen Tech Rep.
483 RMRS-GTR-165. U.S. Department of Agriculture, Forest Service, Rocky Mountain
484 Research Station, Fort Collins, Colorado, USA.

485 Rehfeldt GE, Crookston NL, Warwell MV, Evans JS. 2006. Empirical analyses of plant-climate
486 relationships for the western United States. *International journal plant science* 167:1123–
487 1150. DOI: 1058-5893/2006/16706-0005.

488 Richards JA. 1999. *Remote Sensing Digital Image Analysis*, Springer-Verlag, Berlin, p.240.

489 Riley SJ, Degloria SD, Elliot R. 1999. A terrain ruggedness index that quantifies topographic
490 heterogeneity. *Intermountain Journal of Sciences*5:23–27
491 (http://arcscripts.esri.com/details.asp?dbid=12435).

492 Roberts N, Ezcurra E. Desert Climate. 2012. In: Rebman, JP, Roberts NC, ed. *Baja California*
493 *Plant Field Guide*. San Diego Natural History Museum. San Diego, USA. 1-23.

PeerJ Preprints | https://doi.org/10.7287/peerj.preprints.3439v6 | CC BY 4.0 Open Access | rec: 20 Mar 2018, publ: 20 Mar 2018

494 Rouse JW, Haas RH, Schell A, Deering DW. 1974. Monitoring vegetation systems in the Great
495 Plains with ERTS. Proceedings of the Third Earth Resources Technology Satellite-1
496 Symposium, December 10–15 1974, Greenbelt, MD, NASA, Washington, DC, pp.301–
497 317.

498 Sáenz-Romero C, Rehfeldt GE, Crookston NL, Duval P, St-Amant R, Beaulieu J, Richardson
499 BA. 2010. Spline models of contemporary, 2030, 2060 and 2090 climates for Mexico and
500 their use in understanding climate-change impacts on the vegetation. *Climatic Change*,
501 102:595-623. DOI:10.1007/s10584-009-9753-5.

502 Salas EAL, Valdez R, Michel S. 2017. Summer and winter habitat suitability of Marco Polo
503 argali in southeastern Tajikistan: A modeling approach. *Heliyon* 3(11):e00445.
504 DOI:10.1016/j.heliyon.2017.e00445.

505 Sappington, JM., Longshore, KM., Thompson, D. B. 2007. Quantifying landscape ruggedness
506 for animal habitat analysis: a case study using bighorn sheep in the Mojave Desert. *Journal*
507 *of wildlife management*, *71*(5):1419-1426. DOI: 10.2193/2005-723

508 Satage AR, Salas C. 2007. Interactions of Elevation, Aspect, and Slope in Models of Forest
509 Species Composition and Productivity. *Forest Science* 53:486-492. Available at:
510 http://www.ingentaconnect.com/

511 Silva-Flores R, Pérez-Verdín G, Wehenkel C. 2014. Patterns of tree species diversity in relation
512 to climatic factors on the Sierra Madre Occidental, Mexico. *PloS one 9,* e105034. DOI:
513 10.1371/journal.pone.0105034.

PeerJ Preprints | https://doi.org/10.7287/peerj.preprints.3439v6 | CC BY 4.0 Open Access | rec: 20 Mar 2018, publ: 20 Mar 2018

514 Shirk AJ, Waring K, Cushman S, Wehenkel C, Leal-Sáenz A, Toney C, Lopez-Sanchez CA.
515 2017. Southwestern white pine (*Pinus strobiformis*) species distribution models predict
516 large range shift and contraction due to climate change. *Forest Ecology Management* (in
517 review).

518 Sothe C, Almeida CMD, Liesenberg V, Schimalski MB. 2017. Evaluating Sentinel-2 and
519 Landsat-8 Data to Map Sucessional Forest Stages in a Subtropical Forest in Southern
520 Brazil. *Remote Sensing* 9(8):838. DOI:10.3390/rs9080838.

521 Spasojevic MJ, Bahlai CA, Bradley BA, Butterfield BJ, Tuanmu MN, Sistla S, Wiederholt R,
522 Suding KN. 2016. Scaling up the diversity-resilience relationship with trait databases and
523 remote sensing data: the recovery of productivity after wildfire. *Global Change Biology*
524 22(4):1421–1432. DOI: 10.1111/gcb.13174.

525

526 Tan, S.S., Smeins, FE. 1996. Predicting grassland community changes with an artificial neural
527 network model. *Ecological Modelling* 84(1-3): 91-97. DOI: /10.1016/0304-3800(94)
528 00131-6.

529 Tapias R, Climent J, Pardos JA, Gil L. 2004. Life histories of Mediterranean pines. *Plant*
530 *Ecology* 171: 53-68. DOI:10.1023/B:VEGE.0000029383.72609.f0.

531 Telespazio VEGA Deutschland GmbH 2016. Sentinel-2 MSI-Level-2A. Prototype Processor
532 Installation and User Manual. Available at:
533 http://step.esa.int/thirdparties/sen2cor/2.2.1/S2PAD-VEGA-SUM-0001-2.2.pdf

PeerJ Preprints | https://doi.org/10.7287/peerj.preprints.3439v6 | CC BY 4.0 Open Access | rec: 20 Mar 2018, publ: 20 Mar 2018

534 Tsujino R, Takafumi H, Agetsuma N, Yumoto T. 2006. Variation in tree growth, mortality and
535 recruitment among topographic positions in a warm temperate forest. *Journal of*
536 *Vegetation Science* 17:281-290. DOI:10.1658/1100-
537 9233(2006)17[281:VITGMA]2.0.CO;2.

538 Venables WN, Ripley BD. 2002. Modern Applied Statistics with S-Plus. Fourth Edition. New
539 York, Springer.

540 Vieira ICG, de Almeida AS, Davidson EA, Stone TA, de Carvalho CJR, Guerrero JB. 2003.
541 Classifying successional forests using Landsat spectral properties and ecological
542 characteristics in eastern Amazonia. *Remote Sensing of Environment* 87(4):470-481.
543 DOI:10.1016/j.rse.2002.09.002.

544 Wu W, Li AD, He XH, Ma R, Liu HB., Lv JK. 2018. A comparison of support vector machines,
545 artificial neural network and classification tree for identifying soil texture classes in
546 southwest China. *Computers and Electronics in Agriculture* 144:86-93. DOI:
547 10.1016/j.compag.2017.11.037.